Simulation of propylene polymerization: an efficient algorithm

Priyabrata Sarkar and Santosh K. Gupta*
Department of Chemical Engineering, Indian Institute of Technology, Kanpur-208016, India
(Received 24 September 1990; revised 6 February 1991; accepted 19 March 1991)

Multigrain type models for propylene polymerization suffer from the drawback that they take excessive computer time to predict the degree of polymerization (DP) and the polydispersity index (Q) of the polymer produced. An efficient algorithm using adaptive grid-point spacing in a finite-difference technique has been developed to overcome this defect. Using this algorithm, we have studied the effects of catalyst deactivation as well as multiplicity of catalyst sites, on the rate of polymerization, and on the values of DP and Q. The improved algorithm can easily be used to model industrial reactors where additional physicochemical effects are present.

(Keywords: polymerization; propylene; modelling)

INTRODUCTION

A significant amount of research has been reported on Ziegler–Natta (Z–N) polymerizations in the last two decades. This is particularly so for the polymerization of propylene. Newer developments of high activity catalysts are leading to continuous upgrading of technology and improvement of product physical properties. An interesting feature in the study of propylene polymerization is that there is no universally accepted theory to explain the relatively broad molecular weight distribution (MWD) of the polypropylene formed using some Z–N catalysts, several of which are still being used in industry today. Actual values of the polydispersity index (*PDI* or Q)[1–3] range from about 5 to 30.

A number of theories have been proposed by researchers to explain this phenomenon, and these are discussed in our earlier paper[4]. The polymeric multigrain model (PMGM) was proposed in that paper[4] to predict higher PDIs even with single site and non-deactivating catalysts under certain conditions, and this can be used in the simulation of industrial reactors. However, the computer time required for obtaining results using this model is very high, even for studies on single catalyst particles. This is also true when one uses the multigrain model (MGM) of Floyd *et al.*[5]. The high computational costs put severe limitations on the use of these models for simulation of industrial reactors wherein additional physicochemical phenomena are present, as well as making studies on the optimization and control of such reactors prohibitive. Also, if one were to study the effect of multiple catalyst sites or incorporate diffusional resistances of the chain transfer agent (usually hydrogen), the CPU time would increase further by a few times. Hence, there is a definite need to study approximations and means to reduce computer time without losing significantly in terms of accuracy.

This paper presents a computational algorithm, which we shall refer to as the 'clubbed shell algorithm' (CSA), which is more efficient than our earlier one (EA)[4], as well as that used by Floyd *et al.*[5,6]. We have studied the effect of various parameters on the polymerization of propylene using this algorithm and have compared the results obtained with those using the EA, to see how accurate these results are. The effects of incorporating the diffusional resistance of the chain transfer agent as also that of using multisite catalysts have been studied, something which could not be done earlier due to constraints of computational time.

FORMULATION

The polymeric multigrain model[4] has been developed based on the experimental observation[1] that the catalyst is present as small fragments in a polymer continuum (see *Figure 1*). This conglomerate of polymer and catalyst fragments is called a macroparticle. Monomer diffuses from the liquid medium (bulk) in which the macroparticles lie, to the surface of these macroparticles through the liquid film around them. The following partial differential equation accounting for diffusion as well as reaction, is obtained for the concentration, M, of the monomer at any radial position, r, and time, t, in a single spherical macroparticle:

$$\frac{\partial M}{\partial t} = D_{ef}\frac{1}{r^2}\frac{\partial}{\partial r}\left(r^2\frac{\partial M}{\partial r}\right) - \mathscr{R} \qquad (1a)$$

$$\text{at } r = 0, \quad \frac{\partial M}{\partial r} = 0 \qquad (1b)$$

$$\text{at } r = R_{N+2}, \quad D_{ef}\frac{\partial M}{\partial r} = k_1(M_b - M) \qquad (1c)$$

$$\text{at } t = 0, \quad M = M_b \qquad (1d)$$

Here $\mathscr{R}$ is the net rate of consumption of monomer per

* To whom correspondence should be addressed

0032-3861/92/071477-09

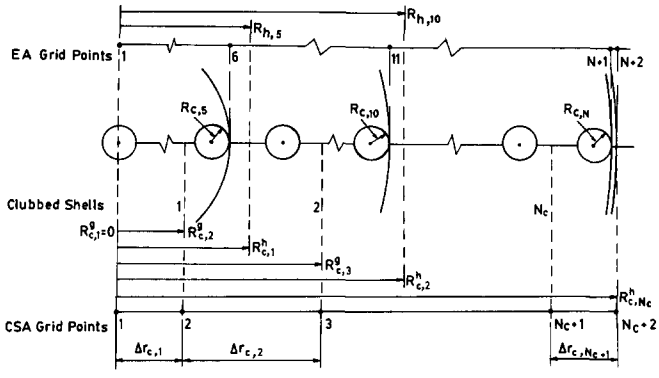

Figure 1 Polymeric multigrain model with clubbing

unit macroscopic volume at any position, R_{N+2} is the radius of the macroparticle, k_1 is the mass transfer coefficient characterizing transfer of the monomer from the bulk, at concentration M_b, to the macroparticle surface, and D_{ef} is the effective monomer diffusivity inside the macroparticle. The other terms are as defined in the Nomenclature. Since, in this model, the catalyst fragments are assumed to be in a continuum of polymer, there is no macroparticle porosity term in equation (1a), in contrast to that in the multigrain model of Floyd *et al.*[6]. However, to account for the resistance due to the presence of the solid catalyst fragments, an effective diffusivity is used in this equation. This coefficient is computed by multiplying the diffusivity, D_1, of monomer through pure polymer with a correction factor equal to the area-fraction (approximated by the volume fraction or alternatively, by (volume fraction)$^{2/3}$) of polymer in the macroparticle at any radial location. Thus, D_{ef} is a function of r as well as t.

The rate term, $\mathscr{R}$, in equation (1a) is computed using the more detailed particulate picture of the macroparticle. The catalyst fragments are assumed to be located in different spherical shells, as shown in *Figure 1*. It is assumed that as polymerization progresses, the polymer produced by the catalyst particles in any shell is accommodated in that shell itself. Thus, the shells not only expand outward with time, but also become thicker. There are $N + 2$ grid points associated with the N shells. The finite difference technique for unequally spaced grid points[7] can be applied at the ith grid point to reduce equation (1a) to a set of $N + 2$ ordinary differential equations (ODEs) for the concentration, M_i, of the monomer at this location. The corresponding rate term, $\mathscr{R}_i$, at this location, can easily be written using the kinetic scheme shown in *Table 1*. $\mathscr{R}_i$ will incorporate M_i. The set of $N + 2$ coupled ODEs for M_i so obtained can easily be integrated with the help of a library subroutine using Gear's technique. It must be emphasized that while carrying out this integration over a time period, Δt, the grid points are assumed to be 'frozen', i.e. the polymer produced in this time interval does not increase the particle (and shell) size. The detailed equations are given in our previous paper[4].

If one were only interested in the monomer concentration profiles in the macroparticles, one could carry out the above integration, and update (accommodate) the polymer produced in each shell after every time interval, Δt (see Appendix 1). However, if one were also interested in obtaining the number average chain length, DP_i, and the polydispersity index, Q_i, of the polymer in each shell as a function of time, as well as their mean values over the entire particle, more detailed equations would be required. Balance equations for $\lambda_{0,i}$, $\lambda_{1,i}$, $\lambda_{2,i}$, $\Lambda_{0,i}$, $\Lambda_{1,i}$, $\Lambda_{2,i}$ and $P_{1,i}$, as given in *Table 1* (equations (f)–(j), (r)) must then be solved for *each* of the N shells. It is easily seen that even for a moderate value of the number of spherical shells, say 20 to 50, the number of ODEs which need to be solved *simultaneously* becomes prohibitively large ($8N + 2$).

We found in our previous work[4] that we can reduce the computational time without sacrificing accuracy of results, if we decouple the equations for M_i from the equations for the seven other variables (moments$_i$ and $P_{1,i}$). We first solve the $N + 2$ ODEs for M_i for a time interval, Δt. Then, we use this monomer concentration

Table 1 Kinetic scheme, rate and moment equations (QSSA[a] used)

Initiation:

$$P_0 + M \xrightarrow{k_p} P_1 \qquad \text{(a)}$$

Propagation:

$$P_n + M \xrightarrow{k_p} P_{n+1} \qquad \text{(b)}$$

Termination:

$$P_n + 1/2H_2 \xrightarrow{k_{tr}} D_n + P_0 \qquad \text{(c)}$$

Material balance[b]:

$$\frac{dP_n}{dt} = k_p M\left[P_{n-1} - \frac{1}{\alpha}P_n\right]; \quad n = 1, 2, \ldots \qquad \text{(d)}$$

$$\frac{dD_n}{dt} = k_p M P_n[1/\alpha - 1]; \quad n = 1, 2, \ldots \qquad \text{(e)}$$

$$\frac{d\lambda_1}{dt} = C_1 - C_4\lambda_1 \qquad \text{(f)}$$

$$\frac{d\lambda_2}{dt} = C_1 + 2C_3\lambda_1 - C_4\lambda_2; \quad \lambda_j \equiv \sum_{n=1}^{\infty} n^j P_n, \quad j = 0, 1, 2, \ldots \qquad \text{(g)}$$

$$\frac{d\Lambda_0}{dt} = C_4(C_5 - C_7) \qquad \text{(h)}$$

$$\frac{d\Lambda_1}{dt} = C_4(\lambda_1 - C_7) \qquad \text{(i)}$$

$$\frac{d\Lambda_2}{dt} = C_4(\lambda_2 - C_7); \quad \Lambda_j \equiv \sum_{n=1}^{\infty} n^j D_n, \quad j = 0, 1, 2, \ldots \qquad \text{(j)}$$

where

$$C_1 = k_p C^* M(3600) \qquad \text{(k)}$$

$$C_2 = (k_p M + k_{tr}H_2^{1/2})(3600) \qquad \text{(l)}$$

$$C_3 = k_p M(3600) \qquad \text{(m)}$$

$$C_4 = k_{tr}H_2^{1/2}(3600) \qquad \text{(n)}$$

$$C_5 = C_1/C_2 \qquad \text{(o)}$$

$$C_7 = C_5(1 - C_3/C_2) \qquad \text{(p)}$$

$$\alpha \equiv \frac{k_p M}{k_p M + k_{tr}H_2^{1/2}} \qquad \text{(q)}$$

[a]Quasi Steady State Approximation (QSSA) applied for λ_0 and P_1 ($d\lambda_0/dt = 0, dP_1/dt = 0$) gives

$$\lambda_0 = C_1/C_2 \qquad \text{(r)}$$

$$P_1 = C_1[C_2 - C_3]/C_2^2 \qquad \text{(s)}$$

The latter has already been substituted in equations (f)–(j)

[b]Subscript i indicating shell number on M, λ_1, λ_2, Λ_0, Λ_1, Λ_2 not indicated

Table 2 Equations for monomer concentration of the CSA

$$\frac{dM_{c,1}}{dt} = \frac{6D_{ef,1}(M_{c,2} - M_{c,1})}{(\Delta r_{c,1})^2} - \mathscr{R}_1 \quad (a)$$

$$\frac{dM_{c,i}}{dt} = \frac{2D_{ef,i}}{\Delta r_{c,i} + \Delta r_{c,i-1}}\left[M_{c,i+1}\left(\frac{1}{\Delta r_{c,i}} + \frac{1}{R^g_{c,i}}\right) - M_{c,i}\left(\frac{1}{\Delta r_{c,i}} + \frac{1}{\Delta r_{c,i-1}}\right) + M_{c,i-1}\left(\frac{1}{\Delta r_{c,i-1}} - \frac{1}{R^g_{c,i}}\right)\right] - \mathscr{R}_i; \quad i = 2, 3, \ldots, N_c + 1 \quad (b)$$

$$\frac{dM_{c,N_c+2}}{dt} = -M_{c,N_c+2}\left[\frac{2k_1}{\Delta r_{c,N_c+1}} + \frac{2D_{ef,N_c+2}}{(\Delta r_{c,N_c+1})^2} + \frac{2k_1}{R^g_{c,N_c+2}}\right] + M_{c,N_c+1}\left[\frac{2D_{ef,N_c+2}}{(\Delta r_{c,N_c+1})^2}\right] + M_b\left(\frac{2k_1}{\Delta r_{c,N_c+1}} + \frac{2k_1}{R^g_{c,N_c+2}}\right) - \mathscr{R}_{N_c+2} \quad (c)$$

$$\mathscr{R}_1 = \mathscr{R}_{N_c+2} = 0 \quad (d)$$

$$\mathscr{R}_i = (3600)k_p C^* M_{c,i}[V^{cat}_{c,i-1}]/[V^s_{c,i-1}] \quad \text{(for single site)} \quad (e)$$

$$\mathscr{R}_i = (3600)(k^1_p C^*_1 + k^2_p C^*_2)M_{c,i}[V^{cat}_{c,i-1}]/[V^s_{c,i-1}] \quad \text{(for two-site)} \quad i = 2, \ldots, N_c + 1 \quad (f)$$

$$D_{ef,1} = D_{ef,N_c+2} = D_1 \quad (g)$$

$$D_{ef,i+1} = \frac{[V^s_{c,i} - V^{cat}_{c,i}]}{V^s_{c,i}} D_1 \quad (h)$$

profile (assuming it to be essentially unchanged during Δt) in the equations for the six moments at point i, and $P_{1,i}$, as well as in the equations for the amount of polymer formed at i, and integrate these equations over time Δt, shell by shell. This algorithm (referred to here as the earlier algorithm, EA), invoking the decoupling of equations, also takes a large CPU time, since one has to solve a set of seven ODEs, N times (one for each shell) after solving $N + 2$ ODEs for M_i (one for each grid point). The need for developing even more efficient computational methods than the EA to solve these equations is, thus, evident.

One possibility which suggests itself is that we club together the spherical shells (computationally), into a lesser number, N_c, of 'clubbed shells', and thus reduce the computational effort. This, in fact, is the essential spirit behind the finite-element and adaptive mesh techniques[7] which have become quite popular in chemical engineering. In fact, we could club together fewer spherical shells in regions where the monomer concentration varies significantly with r, and several shells can be put together where the variation of monomer concentration with location is not as severe, thus reducing computational costs tremendously while not sacrificing numerical accuracy of results.

Indeed, a good test of our present algorithm using clubbing would be the case where the diffusivity of the monomer is low ($D_1 = 0.5 \times 10^{-12}$ to 10^{-12} m^2 s^{-1}). For this case, a steep monomer concentration profile exists[4] near the surface of the macroparticle. The majority of the polymer is formed in these outer shells since a larger number of the catalyst fragments are present there, and the monomer concentration, too, is higher in this zone. The fact that our algorithm (referred to as the clubbed shell algorithm, CSA) satisfies this relatively severe test is proof of its efficacy. *Figure 1* shows how the original shells in the EA are clubbed together. Appendix 1 gives the locations of the grid points to be used in the CSA, as well as the procedure for updating them.

Another improvement in the algorithm is the use of the quasi steady state approximation (QSSA, i.e. $d/dt = 0$) for $P_{1,i}$ and $\lambda_{0,i}$. This leads to algebraic expressions for these variables (instead of ODEs) as given in *Table 1* (equations (r) and (s)). It has also been observed that when values of the diffusivity, D_1, are relatively high (10^{-10} to 5.0×10^{-10} m^2 s^{-1}) the time constants for $\lambda_{1,i}$ are such that the QSSA can be applied to this variable

Table 3 Flow chart for CSA

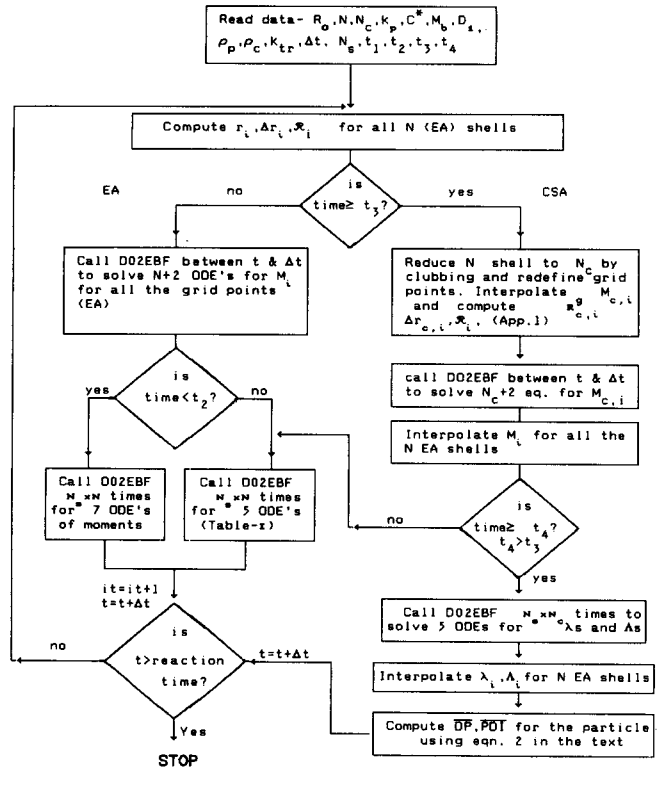

as well (to give $\lambda_1 = C_1/C_4$). This can lead to a further reduction in computer time.

The set of equations to be solved using this CSA is given in *Table 2*. The detailed flow diagram is given in *Table 3*. In the CSA, the EA[4] is used with a larger number, $N + 2$, of grid points, for a short time, $0 \leqslant t \leqslant t_2$, with all seven equations for the moments and P_1 being integrated at each shell. In this interval, a smaller value, Δt_1, is used in $0 \leqslant t \leqslant t_1$, while a larger Δt_2 is used for $t_1 \leqslant t \leqslant t_2$, to avoid oscillations in the results. Thereafter, for $t_2 \leqslant t \leqslant t_3$, the EA is used with the QSSA applied to the equations for $\lambda_{0,i}$ and $P_{1,i}$. In the range $t_3 \leqslant t \leqslant t_4$, clubbing of shells is used to solve a lesser number, $N_c + 2$, of ODEs for the monomer concentration, $M_{c,i}$. The concentration of the monomer at the midpoints of each

of the *original* N shells is then found by linear, polynomial or cubic spline interpolation, depending upon the parameter values. The five moment equations in each of the original N shells are obtained by integration. This information is used to calculate the DP and PDI in each of the original N shells. Finally, for $t > t_4$, the equations for $M_{c,i}$ and the set of five equations for the moments are integrated at $N_c + 2$ and N_c points respectively, i.e. clubbing has been used for the diffusion equation, as well as for the moment equations. The moments are interpolated to give the values in each of the N original shells, and values of DP_i and Q_i are evaluated, along with their particle-average values.

The results obtained using this new algorithm compare well with our earlier results[4], with the advantage that there is a considerable reduction in the computational costs. This enables one to study several other effects at reasonable costs. For example, the algorithm is used to study the effect of multiple catalyst sites on the MWD broadening. In this case the reaction term, $\mathscr{R}$, gets modified. Also, the set of moment equations is solved twice (once for each of the two kinds of catalyst sites considered here) for every monomer concentration profile. DP (or M_n) and PDI ($=Q$) are calculated using the following equations:

$$M_{n,i}^{(k)} = \frac{\lambda_{1,i}^{(k)} + \Lambda_{1,i}^{(k)}}{\lambda_{0,i}^{(k)} + \Lambda_{0,i}^{(k)}} (MW) \tag{2a}$$

$$M_{w,i}^{(k)} = \frac{\lambda_{2,i}^{(k)} + \Lambda_{2,i}^{(k)}}{\lambda_{1,i}^{(k)} + \Lambda_{1,i}^{(k)}} (MW) \tag{2b}$$

$$M_{n,i} = \frac{1}{\sum_{k=1}^{N_s} w_i^{(k)} / M_{n,i}^{(k)}} \tag{2c}$$

$$M_{w,i} = \sum_{k=1}^{N_s} w_i^{(k)} M_{w,i}^{(k)} \tag{2d}$$

$$Q_i = M_{w,i} / M_{n,i} \tag{2e}$$

$$\bar{M}_n = \frac{1}{\sum_{i=1}^{N} w_i / M_{n,i}} \tag{2f}$$

$$\bar{M}_w = \sum_{i=1}^{N} w_i M_{w,i} \tag{2g}$$

$$\overline{PDI} = \bar{Q} = \bar{M}_w / \bar{M}_n \tag{2h}$$

where (k) denotes the kth kind of active site, i denotes the ith shell, w_i^k is the ratio of the mass of polymer produced by the kth site in the ith shell to the mass of polymer produced by all sites in that shell, and w_i is the ratio of the mass of the polymer (from all sites) in the ith shell to that in the entire macroparticle. N_s is the number of types of catalyst sites present.

The effect of diffusion of the chain transfer agent has been neglected in most earlier studies. But in a number of cases this may not be so. For example, if the diffusivity of monomer through the polymer is small, then the monomer concentration in the bulk of the macroparticle becomes quite small and remains so for quite some time. In this region, the concentration of the chain transfer agent (hydrogen) may be even higher than the monomer concentration. This leads to an abnormally high PDI and consequently very low DP in the bulk of the particle. The results are obviously erroneous. However, for moderate or low diffusivity values of the monomer, the effect is negligible. Using our program we have obtained results incorporating the diffusion of hydrogen, taking its diffusivity higher than that of the monomer. In this case, the diffusion equations need to be solved twice (for monomer and hydrogen). The decay of catalyst activity has also been incorporated in this study and interesting results are obtained.

The CS algorithm thus provides a wide range of choices in the simulation of polypropylene reactors at low computational costs.

RESULTS AND DISCUSSION

A reference set of values for the parameters is chosen and results obtained using both the EA and from the CSA are compared. These parameters are given in *Table 4*. It has been assumed in the reference run that the catalyst fragments are of the same size in each shell. The parameters are selected so as to have relatively severe diffusional limitations ($D_1 = 10^{-12}$ m^2 s^{-1}) in a moderate sized catalyst particle (initial radius of the catalyst particle before fragmentation, $R_0 = 1.15 \times 10^{-5}$ m). This was done purposely to show that even with a relatively steep monomer concentration profile (see *Figure 2*), the clubbed shell algorithm predicts values of $\overline{DP}$, $\bar{Q}$ and rate of polymerization (*Figure 3*) which are close to those obtained by the EA. One notes, therefore, that even for the reference conditions the CSA works fairly well. The CPU time taken for the reference CSA run was only 7 s on a supermini HP9000/850S as compared to 87 s using the EA. CPU times for other cases studied are given in *Table 5*. It is evident from *Figures 2* and *3* that values of $\overline{DP}$ and $\bar{Q}$ are more sensitive to the use of CSA, than are the monomer profiles or rate of polymerization.

We also tried using effective diffusivity = $D_1 \times$ (volume fraction of polymer)$^{2/3}$, instead of $D_1 \times$ (volume fraction). *Figure 3* shows that this leads to slightly lower values of $\overline{DP}$ and $\bar{Q}$ in the early stages of polymerization only. The rate and monomer profiles are quite insensitive to the form of the equation used for the effective diffusivity.

Table 4 Reference values of the parameters and conditions

Parameter	Value	
D_1	1×10^{-12}	m^2 s^{-1}
M_b	4.0×10^3	mol m^{-3}
R_0	1.15×10^{-5}	m
$R_{c,i}$	2.0×10^{-7}	m
C^*	1.0	mol site (m^3 cat)$^{-1}$
k_p	0.50	m^3 mol site^{-1} s^{-1}
k_{tr}	0.186	m$^{3/2}$ mol$^{-1/2}$ s^{-1}
H_2	1.0	mol m^{-3}
k_1	1.0×10^{-3}	m s^{-1}
N	36	
N_c	9 (five original shells in each of the inner six clubbed shells, two in each of outer three shells)	
ρ_P	900	kg m^{-3}
ρ_c	2260	kg m^{-3}
Interpolation		Linear
Computational parameters:		
Δt_1	10^{-4}	h
Δt_2	10^{-3}	h
t_1	0.002	h
t_2	0.005	h
t_3	0.24	h
t_4	0.25	h
Tol	0.0001	

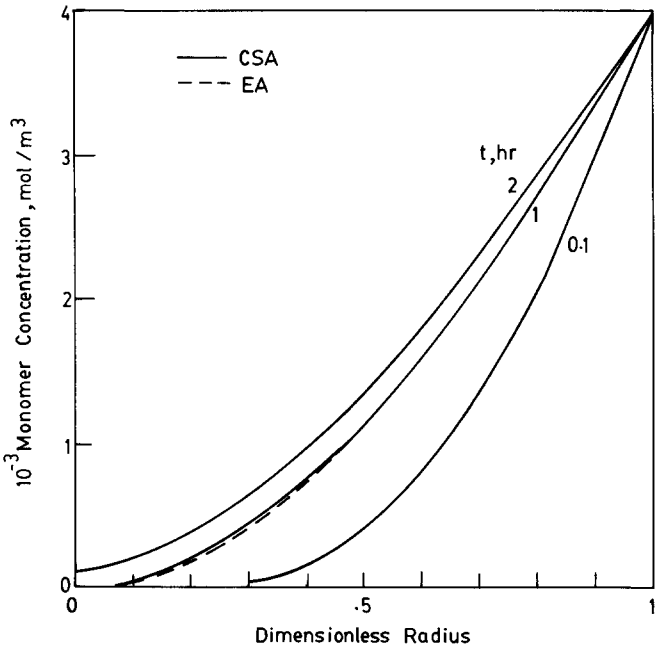

Figure 2 Comparison of monomer concentration profiles with (——) and without (– – –) clubbing at 0.1 h, 1 h and 2 h. Reference values of parameters used. No difference between EA and CSA results seen for $t = 0.1$ and 2 h

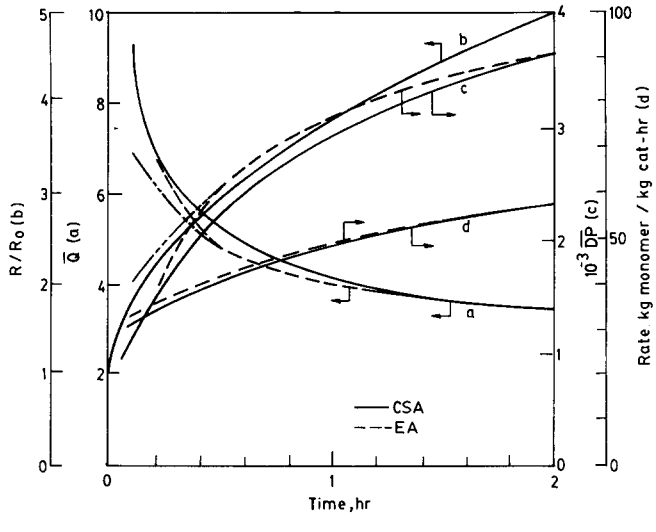

Figure 3 Comparison of $\bar{Q}$ (a), R/R_0 (b), $\overline{DP}$ (c) and rate (d) obtained with (——) and without (– – –) clubbing. Reference values of parameters used. ——— shows results when $D_1 \times$ (volume fraction)$^{2/3}$ is used to estimate effective diffusivity

For moderate values of the diffusivity ($D_1 = 10^{-11}$ m^2 s^{-1}), and with $k_P = 1$ m^3 mol^{-1} s^{-1} and $H_2 = 1.5$ mol m^{-3}, one can use $\Delta t_1 = \Delta t_2 = 0.001$ h, $t_1 = t_2 = 0.002$ h, $t_3 = 0.004$ h, $t_4 = 0.004$ h, i.e. we switch over to clubbing for both monomer and the moment equations quite soon, without sacrificing accuracy (see *Figure 4*). These conditions are more typical of real systems. Results for the case when the radii of the catalyst fragments in the different shells are randomly[8] distributed (average value = 2×10^{-7} m, $R_{max} = 2.5 \times 10^{-7}$ m, but with R_0 = reference value) and $D_1 = 10^{-11}$ m^2 s^{-1}, $k_P = 1$ m^3 mol^{-1} s^{-1}, $H_2 = 1.5$ mol m^{-3}, are also shown in this figure. It is observed that the introduction of particle size distribution leads to only slight increases in $\overline{DP}$ and rate of polymerization. For even higher values of D_1 (10^{-10}–10^{-11} m^2 s^{-1}), results generated with $\Delta t_1 = \Delta t_2 = 0.01$ h, and $t_1 = t_2 = t_3 = t_4 = 0.01$ h are quite accurate. The CPU time falls drastically to about 0.6 s. Use of $D_1 \times$ (volume fraction)$^{2/3}$ for the effective diffusivity leads only to imperceptible changes in all these results.

The effect of deactivation of the catalyst has been examined using this improved algorithm. First-order deactivation of the catalyst, described by

$$k_P(t) = k_P^0 \exp(-t/\lambda') \tag{3a}$$

$$t_{1/2} = \lambda' \ln 2 \tag{3b}$$

is used. In equation (3), k_P^0 is the catalyst activity at $t = 0$, and λ' is the first-order deactivation constant related to the half-life, $t_{1/2}$. Results are shown in *Figures 5* and *6*. CSA results for the reference run are shown henceforth, wherever presented. It is seen that the *PDI* shows an increase after an initial fall for highly deactivating catalysts. A similar observation was made by Keii *et al.*[9]. $\overline{DP}$ shows a maxima for such systems, at about the same time as $\bar{Q}$ shows a minimum. *Figure 6* shows that deactivation leads to a maximum in the polymerization rate (decay type behaviour[10]) as opposed to acceleration type behaviour[10] (curve a) in the absence of catalyst decay. Values of $\bar{Q}$ are observed to go up to about six.

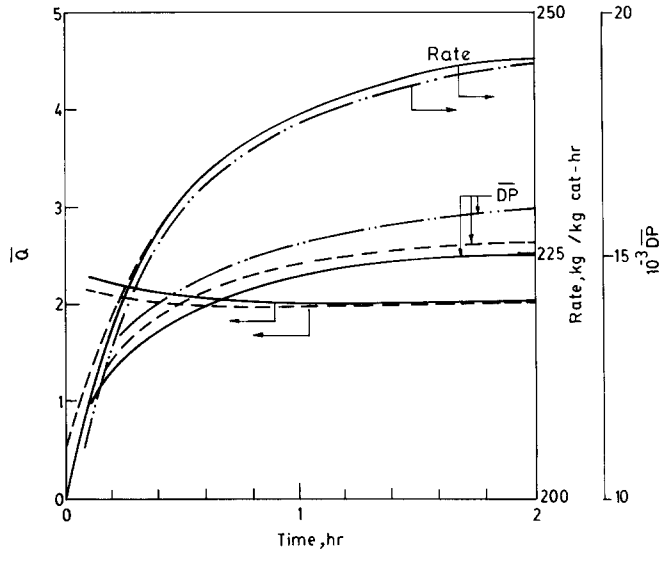

Figure 4 Comparison of $\bar{Q}$, $\overline{DP}$ and rate with (——) and without (– – –) clubbing for $D_1 = 1 \times 10^{-11}$ m^2 s^{-1}, $k_P = 1$ m^3 mol site^{-1} s^{-1}, and $H_2 = 1.5$ mol m^{-3}. Other parameters are the same as reference values. Results with radius of the catalyst fragments randomly chosen (mean radius = 2×10^{-7} m) and $D_1 = 10^{-11}$ m^2 s^{-1}, $k_P = 1$ m^3 mol site^{-1} s^{-1} also shown (— · · —). $\bar{Q}$ for the latter are indistinguishable from CSA values

Table 5 CPU time (HP9000/850S) for the reference run

Algorithm	CPU time (s)
EA (without QSSA, single site)	110
EA (with QSSA, single site)	87
EA (with QSSA, double site)	150
CSA (without QSSA, single site)	25
CSA (with QSSA, single site)	7
CSA (with QSSA, double site)	11

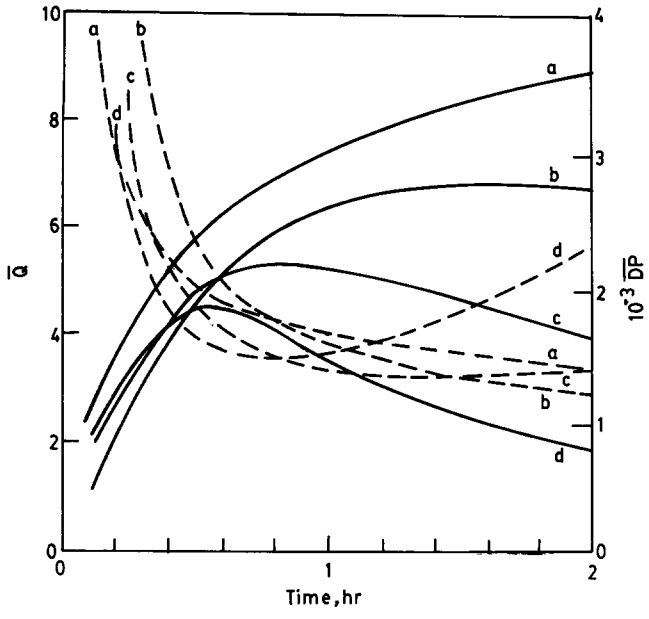

Figure 5 Effect of first order deactivation of catalyst on $\bar{Q}$ (---) and $\overline{DP}$ (——); (a) no deactivation; (b) $t_{1/2} = 1.5$ h; (c) $t_{1/2} = 0.5$ h; (d) $t_{1/2} = 0.25$ h. CSA results for (a) shown

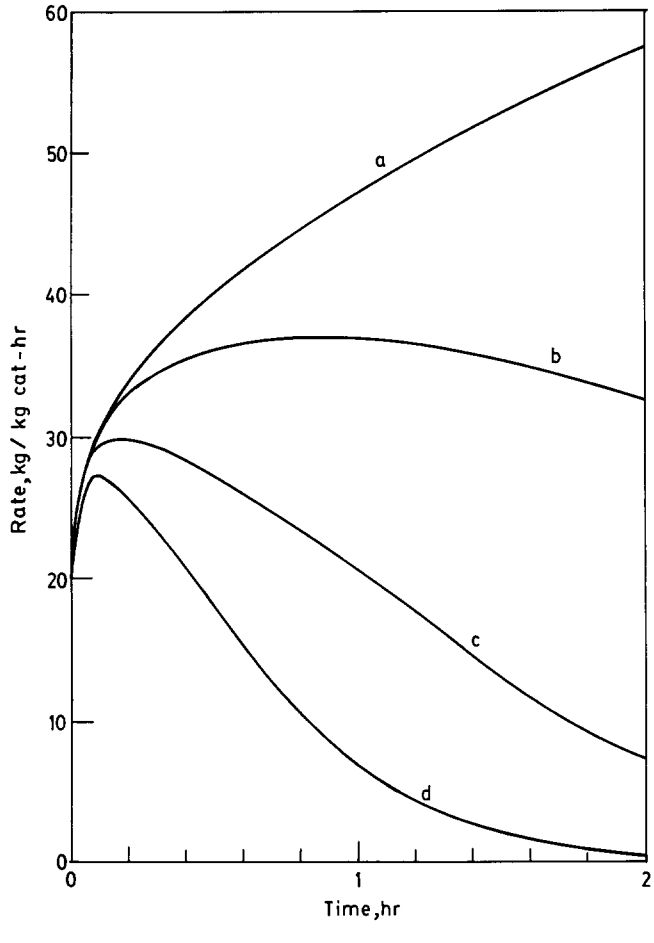

Figure 6 Effect of first order decay on the rate of polymerization: (a) no deactivation; (b) $t_{1/2} = 1.5$ h; (c) $t_{1/2} = 0.5$ h; (d) $t_{1/2} = 0.25$ h

Another interesting point of investigation is to see the effect of hydrogen (chain transfer agent) diffusion in the polymer particle. Many researchers[11] have mentioned this phenomenon, but so far the effect has not been investigated quantitatively. For low values of D_1 or high values of R_0, it was observed (*Figure 2*) that the values of M_i near the centre of the macroparticle are quite small. In fact, in this region, M_i is even lower than the concentration of hydrogen (assumed constant in the reference run). The values of DP obtained in this region are less than one, and do not represent realistic values. *Figure 7* shows the values of $\bar{Q}$ and $\overline{DP}$ for three different values of hydrogen diffusivity, D_h. It may be noted that if we increase the hydrogen concentration keeping D_h constant (at ∞, curve d, *Figure 7*), $\overline{DP}$ decreases substantially, while $\bar{Q}$ increases to some extent. This leads us to the observation that one can control $\overline{DP}$ keeping $\bar{Q}$ essentially unchanged, by changing the concentration of the chain transfer agent.

One of the more important parameters is the initial catalyst radius (before fragmentation), R_0. Yet, it is surprising that earlier researchers have not studied the effect of changing this parameter. If we examine *Figure 8*, we see that a small change in the initial catalyst radius from 10 μm to 13 μm changes the product $\bar{Q}$ from 3 to 4.8, and $\overline{DP}$ drops from about 4600 to 2500. Also, both the growth rate and the rate of polymerization decrease considerably. Thus, we conclude that the average catalyst particle size plays an important role in deciding whether the polymerization process becomes diffusionally limited or not. In fact, it can be shown that with a monomer diffusivity as high as 0.5×10^{-10} m^2 s^{-1} and a catalyst radius of 20 μm (reference value 11.5 μm), a $\bar{Q}$ higher than 2 can be obtained.

The CSA has enabled us to investigate the effect of using a catalyst with multiple activity sites. *Table 5* indicates that the CPU time with two catalyst sites is only 11 s. Many researchers[12–17] have concluded that multisite activity catalysts are the main reason for the excessive breadth of the MWD. In order to compare the

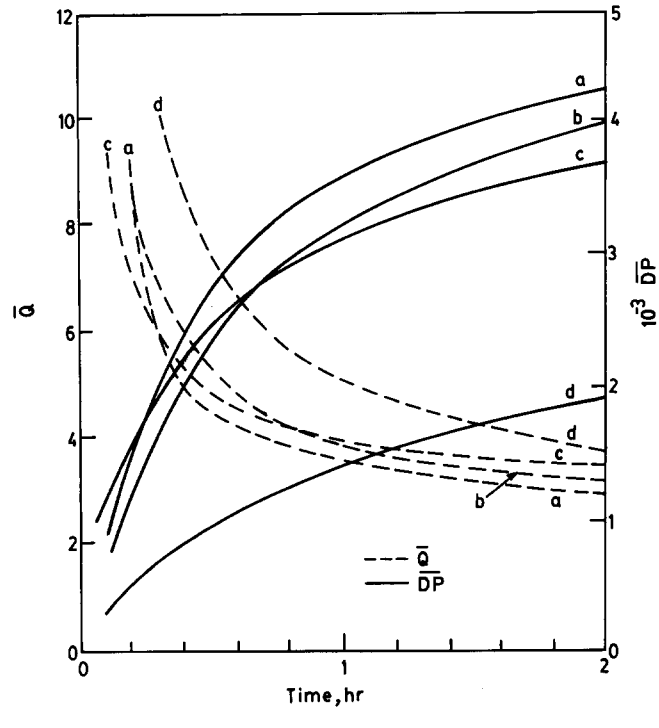

Figure 7 Effect of diffusion of hydrogen on $\bar{Q}$ (---) and $\overline{DP}$ (——) with (c) $D_h = \infty$ (reference); (b) $D_h = 1.0 \times 10^{-11}$ m^2 s^{-1}; (a) $D_h = 5.0 \times 10^{-12}$ m^2 s^{-1}. Hydrogen concentration = 1.0 mol m^{-3}. Results for hydrogen concentration of 3.0 mol m^{-3} with $D_h = \infty$ also shown (curves d)

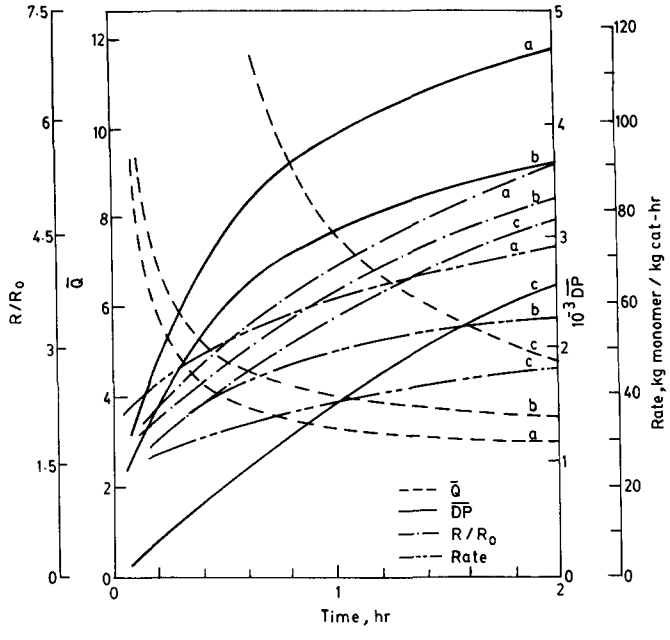

Figure 8 Effect of initial (unfragmented) catalyst radius (R_0) on $\bar{Q}$, $\overline{DP}$, R/R_0 and rate of polymerization. R_0 = (a) 1×10^{-5} m; (b) 1.15×10^{-5} m (ref.); (c) 1.3×10^{-5} m

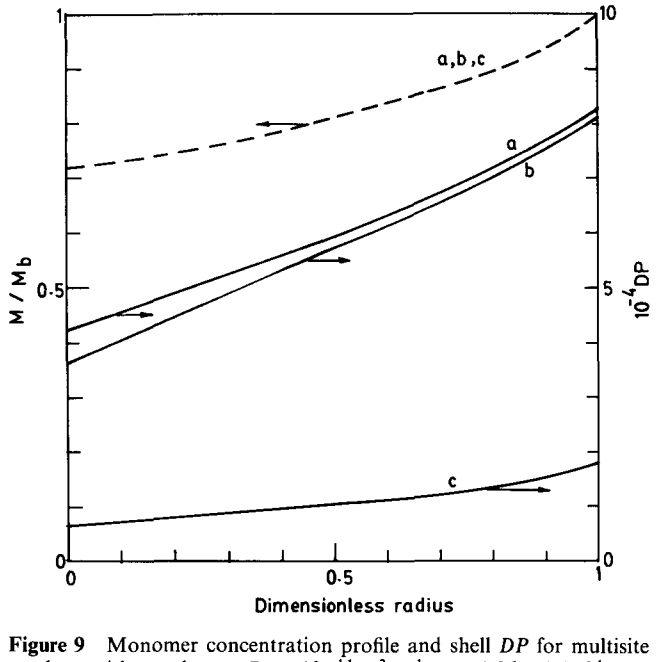

Figure 9 Monomer concentration profile and shell DP for multisite catalyst without decay. $D_1 = 10^{-11}$ m^2 s^{-1}, $t = 1.0$ h. (a) $k_P^1 = 3$, $k_P^2 = 7$, $C_1^* = 0.1$, $C_2^* = 0.1$; (b) $k_P^1 = 1$, $k_P^2 = 9$, $C_1^* = 0.1$, $C_2^* = 0.1$; (c) $k_P^1 = 0.5$, $k_P^2 = 5$, $C_1^* = 1$, $C_2^* = 0.1$. k_P are in m^3 mol site^{-1} s^{-1} and C^* are in mol site m^{-3}

results of the multisite with those of the single site catalyst, we have obtained results using $(k_P^1 C_1^* + k_P^2 C_2^*)$ to be the same as the $k_P C^*$ value for the single site catalyst. This was done to obtain similar monomer concentration profiles for the two cases (see *Figure 9*). The monomer diffusivity has been taken as 10^{-11} m^2 s^{-1} (instead of 10^{-12} m^2 s^{-1} as for the reference run). This value is taken since the single site catalyst gives values of $\bar{Q}$ close to 2 under these conditions. It is observed that even though the three multisite catalysts considered (cases a, b, c) lead to similar monomer concentration profiles in the macroparticle (*Figure 9*), the values of $\overline{DP}$ and $\bar{Q}$ (*Figure 10*) differ substantially. The larger is the difference in the k_P^i values, the higher are the values of $\bar{Q}$, and the lower are the values of $\overline{DP}$. We also generated results using different C_i^* ($\sum k_P^i C_i^*$ is not the same) but keeping k_P^1 and k_P^2 unchanged. Again, significant differences in $\overline{DP}$ and $\bar{Q}$ are observed. *Figure 10* shows how the introduction of multisite activity of the catalyst leads to higher values of $\bar{Q}$ than predicted under similar conditions for single activity catalysts. *Figure 10* also shows the effect of deactivation on the polymerization of propylene with multisite catalysts. Even further increases in the values of $\bar{Q}$ are observed.

CONCLUSIONS

The polymeric multigrain model has been made computationally more efficient by using clubbing of shells. The algorithm is then used for analysis of the effects of the diffusion of the chain transfer agent, multiple site activity of the catalyst, deactivation of the catalyst, etc. The CPU times are reduced substantially. The algorithm can now be used for the simulation of different types of polypropylene reactors (e.g. continuous liquid slurry, liquid pool or fluidized bed) where additional physicochemical effects are present, and more extensive computations are necessary. This work is in progress. Analysis of the effects of the various parameters reveals that:

(1) With single site catalysts, larger initial catalyst particles can give rise to high PDIs even with higher monomer diffusivities.

(2) With single site catalysts, high deactivation rates can result in broader MWDs and decay type rate curves.

(3) The effect of catalyst fragment size distribution is *relatively* unimportant provided the initial size of the macroparticle is the same.

(4) Multisite catalysts can produce polymer with high PDIs, even with high monomer diffusivities.

REFERENCES

1 Buls, V. W. and Higgins, T. L. *J. Polym. Sci., Polym. Chem. Edn.* 1970, **8**, 1025

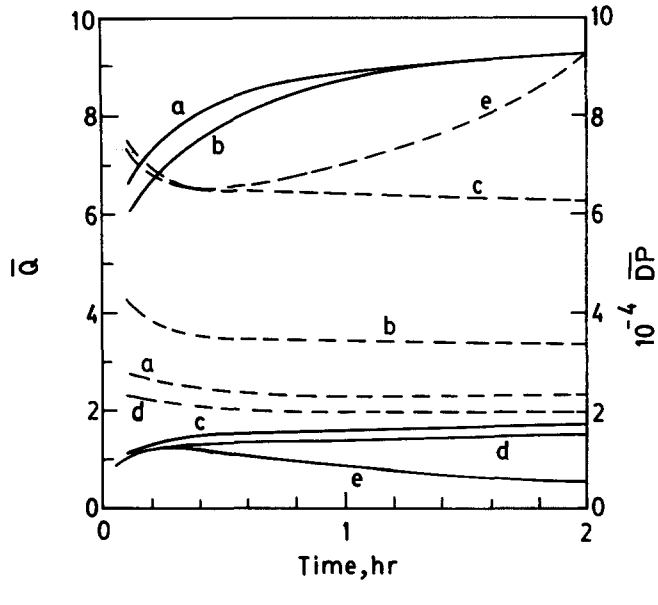

Figure 10 Effect of k_P^i and C_i^* on $\bar{Q}$ (---) and $\overline{DP}$ (——) for two-site catalyst. a, b, c as in *Figure 9*; (d) single-site catalyst, $k_P = 1.0$, $C^* = 1.0$; (e) case c with $t_{1/2} = 0.5$ h for both sites

2 Crabtree, J. R., Grimsby, F. N., Nummelin, A. J. and Sketchley, J. M. *J. Appl. Polym. Sci.* 1973, **17**, 959
3 Vanderberg, E. J. and Repka, B. C. in 'Polymerization Processes' (Eds. C. E. Schildknecht and I. Skeist), Wiley, New York, 1977
4 Sarkar, P. and Gupta, S. K. *Polymer* 1991, **32**, 2842
5 Floyd, S., Heiskanen, T., Taylor, T. W., Mann, G. E. and Ray, W. H. *J. Appl. Polym. Sci.* 1987, **33**, 1021
6 Floyd, S., Choi, K. Y., Taylor, T. W. and Ray, W. H. *J. Appl. Polym. Sci.* 1986, **32**, 2935
7 Finlayson, B. A. 'Nonlinear Analysis in Chemical Engineering', McGraw-Hill, New York, 1980
8 Nagel, E. J., Kirillov, V. A. and Ray, W. H. *Ind. Eng. Chem., Prod. Res. Dev.* 1980, **19**, 372
9 Keii, T., Doi, Y., Suzuki, E., Tamura, M., Murata, M. and Soga, K. *Makromol. Chem.* 1984, **185**, 1537
10 Keii, T. 'Kinetics of Ziegler Natta Polymerization', Kodansha Sci., Tokyo, 1972
11 Buls, V. W. and Higgins, T. L. *J. Polym. Sci. A-1* 1970, **8**, 1037
12 Bohm, L. L. *Makromol. Chem.* 1981, **182**, 3291
13 Barbe, P. C., Noristi, L., Baruzzi, G. and Marchetti, E. *Makromol. Chem., Rapid Commun.* 1983, **4**, 249
14 Chien, J. C. W. and Hsieh, J. T. T. *J. Polym. Sci., Polym. Chem. Edn.* 1976, **14**, 1915
15 Galvan, R. and Tirrell, M. *Chem. Eng. Sci.* 1986, **41**, 2385
16 Galvan, R. and Tirrell, M. *Comp. Chem. Eng.* 1986, **10**, 77
17 Floyd, S., Heiskanen, T. and Ray, W. H. *Chem. Eng. Progress.* 1988, **84**, 56

NOMENCLATURE

C^* Catalyst active site concentration ($=\lambda_0 + P_0$) (mol m^{-3} catalyst)
C_i^* Catalyst active site concentration for site i (mol m^{-3} catalyst)
$D_{ef,i}$ Effective macroparticle diffusivity at ith grid point (m^2 s^{-1})
D_n Concentration of dead polymer chains having n monomer units (mol m^{-3} catalyst)
D_1 Monomer diffusivity in pure polymer (m^2 s^{-1})
DP Degree of polymerization
H_2 Hydrogen concentration (uniform inside macroparticle) (mol m^{-3})
k_P^i Propagation rate constant for site i (m^3 mol^{-1} s^{-1})
k_l Liquid film mass transfer coefficient (m s^{-1})
k_{tr} Chain transfer rate constant for H_2 (m$^{3/2}$ mol$^{-1/2}$ s^{-1})
M_i Monomer concentration in the large particle at the ith grid point (in EA) (mol m^{-3})
$M_{c,i}$ Monomer concentration in the large particle at the ith grid point (in CSA) (mol m^{-3})
M_b Bulk monomer concentration (mol m^{-3})
$M_{n,i}^{(k)}$ Number average molecular weight of polymer produced by the kth catalyst site in the ith shell
$M_{n,i}$ Number average molecular weight of polymer in the ith shell
$\bar{M}_n$ Mean number average molecular weight of polymer in the macroparticle
$M_{w,i}^{(k)}$ Weight average molecular weight of polymer in the ith shell produced by the kth catalyst site
$\bar{M}_w$ Mean weight average molecular weight of polymer in the macroparticle
MW Molecular weight of monomer (g mol^{-1})
N Number of EA shells
N_c Number of clubbed shells
N_i Number of catalyst fragments in ith shell (in EA)
P Concentration of empty sites (mol m^{-3} catalyst)
P_n Concentration of sites with a growing chain of n monomer units attached (mol m^{-3} catalyst)
$\bar{Q}$ Mean polydispersity index of polymer in the macroparticle
r Radial position (m)
R Radius of macroparticle at any time (m)
$\bar{R}$ Average radius of catalyst fragments (m)
$R_{c,i}$ Radius of catalyst fragment in ith shell, by random number generation (m)
R_0 Initial (unfragmented) catalyst particle radius (m)
$\mathscr{R}_i$ Rate of reaction per unit volume at ith grid point of the clubbed shell (mol m^{-3} h^{-1})
t Time (h)
$V_{c,i}^{cat}$ Volume of catalyst in the ith clubbed shell (m^3)
$V_{c,i}^{s}$ Volume of the ith clubbed shell (m^3)

Greek letters

α Probability of propagation
λ Moment of live polymer
$(P_n)\ \mathrm{MWD}\left(\lambda_k = \sum_{n=1}^{\infty} n^k P_n\right)$
Λ Moment of dead polymer
$(D_n)\ \mathrm{MWD}\left(\Lambda_k = \sum_{n=1}^{\infty} n^k D_n\right)$
ρ_c Density of catalyst (kg m^{-3})
ρ_P Density of polymer (kg m^{-3})
ε^* Void fraction for closed packed spheres (0.476)

APPENDIX 1. SUMMARY OF EQUATIONS USED

Earlier algorithm (see ref. 4 for more details)

$$N_1 = 1 \qquad \text{(A1.1)}$$

$$N_i = 6(1-\varepsilon^*)\left[R_{c,i} + 2\sum_{j=2}^{i-1} R_{c,j} + R_{c,i}\right]^2 \Big/ R_{c,i}^2; \quad i = 2, 3, \ldots, N \qquad \text{(A1.2)}$$

$$\Delta V_i = 3.6 k_P C^* M_{i+1}\left(N_i \frac{4\pi}{3} R_{c,i}^3\right)(MW)(\Delta t)/\rho_P; \quad i = 1, 2, \ldots, N \qquad \text{(A1.3)}$$

$$V_i(t+\Delta t) = V_i(t) + \Delta V_i;$$
$$V_i(t=0) = (4\pi R_{c,i}^3/3) N_i/(1-\varepsilon^*); \quad i = 1, 2, \ldots, N \qquad \text{(A1.4)}$$

$$R_{h,0} = 0; \qquad 4\pi R_{h,i}^3/3 = \sum_{j=1}^{i} V_j; \quad i = 1, 2, \ldots, N \qquad \text{(A1.5)}$$

$$\text{Rate} = \frac{3.6(MW) k_P C^* \sum_{i=1}^{N} (N_i R_{c,i}^3 M_{i+1})}{\rho_c \sum_{i=1}^{N} N_i R_{c,i}^3} \qquad \text{(A1.6)}$$

Clubbing of EA shells

The N EA shells are grouped into larger clubbed shells. The first six clubbed shells contain five EA shells each, while the outer three clubbed shells contain two EA shells each for ($N = 36$, see *Figure 1*). Again, the concept of hypothetical spheres of radius, $R_{c,i}^h$ is proposed. A hypothetical clubbed shell, $R_{c,i-1}^h \leqslant r \leqslant R_{c,i}^h$, is such that it accommodates all the polymer (and catalyst) produced by the catalyst fragments inside it. It is easy to see that

$R^{h}_{c,i}$ is related to $R_{h,i}$:

$$\begin{aligned} R^{h}_{c,i} &= R_{h,5i}; \qquad i = 1, 2, \ldots, 6 \\ R^{h}_{c,7} &= R_{h,32} \\ R^{h}_{c,8} &= R_{h,34} \\ R^{h}_{c,9} &= R_{h,36} \end{aligned} \tag{A1.7}$$

The finite difference grid points in the CSA are assumed to be placed at the mid points of the hypothetical clubbed shells (see *Figure 1*). The grid point locations are thus given by:

$$\begin{aligned} R^{g}_{c,1} &= 0 \\ R^{g}_{c,2} &= R^{h}_{c,i}/2 \\ R^{g}_{c,i+1} &= R^{h}_{c,i-1} + (R^{h}_{c,i} - R^{h}_{c,i-1})/2; \qquad i = 2, 3, \ldots, N_c \\ R^{g}_{c,N_c+2} &= R^{h}_{c,N_c} \end{aligned} \tag{A1.8}$$

and the distances between the grid points (which also change with time) are given by:

$$\begin{aligned} \Delta r_{c,1} &= R^{h}_{c,1}/2 \\ \Delta r_{c,i} &= R^{g}_{c,i+1} - R^{g}_{c,i}; \qquad i = 2, 3, \ldots, N_c + 1 \end{aligned} \tag{A1.9}$$

The volume, $V^{cat}_{c,i}$, of the catalyst in any clubbed shell is obtained by adding up the corresponding volumes in the individual EA shells which are clubbed together:

$$V^{cat}_{c,i} = \sum_{j=n_1(i)}^{n_2(i)} 4\pi R^{3}_{c,j} N_j/3; \qquad i = 1, 2, \ldots, N_c \tag{A1.10}$$

where $n_1(i)$ and $n_2(i)$ indicate the EA shell numbers contained in the ith clubbed shell. Similarly, the volume (polymer and catalyst), of the ith clubbed shell is given by

$$\begin{aligned} V^{s}_{c,1} &= 4\pi(R^{h}_{c,1})^3/3 \\ V^{s}_{c,i} &= 4\pi[(R^{h}_{c,i})^3 - (R^{h}_{c,i-1})^3]/3; \qquad i = 2, 3, \ldots, N_c \end{aligned} \tag{A1.11}$$

In the clubbed shell algorithm, in the time interval $t_3 \leqslant t \leqslant t_4$, the ODEs in *Table 2* for $M_{c,i}$ ($i = 1, 2, \ldots, N_c + 2$), are integrated between time t and $t + \Delta t$, assuming that the shells do not grow in that interval. The values of M_i are then obtained at the mid points of the *EA shells* by interpolation, and equations (A1.3) and (A1.4) are used to obtain the amount of polymer formed in each of the EA shells. The values of $R_{h,i}$ for the EA shells are obtained using equation (A1.5). Equation (A1.7) can then be used to get the new locations of the clubbed shells. In between these computations, the moment equations in *Table 1* are solved in *each* of the EA shells, using interpolated M_i. For $t \geqslant t_4$, both the equations for $M_{c,i}$ and the moments are obtained at the clubbed-shell grid points. The monomer concentration is obtained at the EA grid points by interpolation, and the new values of $R_{h,i}$, etc. obtained as earlier for $t_3 \leqslant t \leqslant t_4$. The moments at the clubbed shell grid points are then interpolated to give values at the *EA grid points*. These are used along with the amount of polymer present in each of *these* EA shells to obtain $M_{n,i}$, $M_{w,i}$, Q_i, etc., and their particle-average values.